

## Polar Kerr effect in multiband spin-orbit coupled superconductors

Meghdad Yazdani-Hamid <sup>1</sup>, Mehdi Biderang <sup>2,3</sup> and Alireza Akbari <sup>3,4,5</sup>


<sup>1</sup>*Department of Physics, Faculty of Sciences, Bu-Ali Sina University, 65178, 016016, Hamedan, Iran*

<sup>2</sup>*Department of Physics, University of Toronto, 60 St. George Street, Toronto, Ontario M5S 1A7, Canada*

<sup>3</sup>*Asia Pacific Center for Theoretical Physics (APCTP), Pohang, Gyeongbuk, 790-784, Korea*

<sup>4</sup>*Institut für Theoretische Physik III, Ruhr-Universität Bochum, D-44801 Bochum, Germany*

<sup>5</sup>*Max Planck POSTECH Center for Complex Phase Materials, and Department of Physics, POSTECH, Pohang, Gyeongbuk 790-784, Korea*

 (Received 25 October 2023; revised 18 January 2024; accepted 20 February 2024; published 13 March 2024)

We undertake a theoretical analysis to probe the Kerr spectrum within the superconducting phase of strontium ruthenate, where the Kerr rotation experiments demonstrate the existence of a superconducting state with broken time-reversal symmetry. We find that spin-orbit coupling changes the hybridization along the Fermi surface's diagonal zone mainly affects Hall transport. We show that the dominant Hall response arises mainly from the quasi-1D orbitals  $d_{yz}$  and  $d_{xz}$ , linked to their hybridization, while other contributions are negligible. This shows that breaking of time-reversal symmetry of quasi-1D orbitals can account for the existence of the Kerr angle, irrespective of the order symmetry specific to the  $d_{xy}$  orbital. Moreover, the optical Hall conductivity and Kerr angle estimated for the hypothesized superconducting orders also closely match the experimental findings, providing important insight on the role of the spin-orbit coupling, hybridization, and emergent order.

DOI: [10.1103/PhysRevB.109.094510](https://doi.org/10.1103/PhysRevB.109.094510)

### I. INTRODUCTION

Despite extensive efforts and a multitude of precise experiments, the true nature of the superconducting order parameter in  $\text{Sr}_2\text{RuO}_4$  continues to elude a definitive answer [1–16]. From an alternative perspective, there is no single comprehensive universal order parameter that can explain all of those outcomes of conducted experiments. For more than two decades, its superconductivity state has been viewed as a two-dimensional analogy to the super-fluid state of  $^3\text{He}$ , namely two-dimensional  $p_x + ip_y$  (a time-reversal symmetry-breaking superconducting state due to spontaneous magnetic fields) [17]. The initial report of the nuclear magnetic resonance (NMR) measurement of the Knight shift [18] and the existence of a nonzero Kerr angle [19] are known as two strong experimental evidences that support this proposed superconducting pairing. However, the lack of edge currents [20] and the absence of a cusp in the strain dependency of  $T_c$  [21,22] exclude this odd-parity pairing state. The more recent NMR experiments have been shown to be inconsistent with triplet pairings and have revealed that the dominant pairings have spin-singlet character and suggest time-reversal symmetry-breaking linear combinations of extended  $s$ -wave [23].

One of the main reasons for the aforementioned longstanding issue is the multi-orbital nature of  $\text{Sr}_2\text{RuO}_4$  that hampers the identification of active and passive bands for the superconducting pairing. The quasi-2D nature of the electronic dispersion introduces these two classes and represents that the superconducting order is derived from either the quasi-2D orbital  $d_{xy}$  or the quasi-1D orbitals  $d_{xz}$  and  $d_{yz}$  [24]. Two classes possess fully different Fermi surfaces such that for the former case, it is isotropic (one circular Fermi surface) whereas for the latter the resulting Fermi surface is highly anisotropic due

to near degeneracies and avoided crossings of different bands. Some thermodynamic and transport properties may favor the first class as the active band and others the second one. For example, the model used under biaxial or uniaxial pressure is based on the first band class because Lifshitz transition occurs for the quasi-2D orbital  $d_{xy}$  whose van Hove peak is nearest to the Fermi surface and have an isotropic Fermi sheet [25–28]. The anisotropic Fermi surfaces of the quasi-1D orbitals  $d_{xz}$  and  $d_{yz}$  with the hybridization gives rise to a finite Berry curvature, which have a close connection with Hall-type response [29,30]. In fact, Berry curvature is associated with the orbital hybridization. Taking into account spin-orbit coupling (SOC) provides a spin-dependent hybridization between three orbitals and gives rise to mixing two classes. Thus one can expect that SOC has profound effects on the Hall-type responses [29].

There are additional supporting evidences indicating the predominant involvement of quasi-1D orbitals, namely from inelastic neutron scattering studies [31], exact weak-coupling analysis of the Hubbard model [32], and tunneling spectroscopy results [33]. Nevertheless, it is noteworthy that these orbitals seem to exert minimal influence on heat capacity measurements [34] and remain relatively unaffected when subjected to strain [26]. This can be attributed to the proximity of the  $d_{xy}$  orbital to the van Hove singularity. Consequently, it becomes increasingly evident that the quasi-1D orbitals play a pivotal role, at the very least, in governing the intrinsic anomalous Hall transport. Identifying these quasi-1D orbitals as the primary active entities also elucidates the absence of edge currents [35–37].

Exploring the intrinsic Hall response of the superconducting state in  $\text{Sr}_2\text{RuO}_4$  in the presence of SOC holds significant interest. Thus far, the investigation of this phenomenon has employed specific methodologies, delineated into two

categories: (i) single-orbital models, where the presence of impurities is crucial as an extrinsic mechanism to induce Hall transport [38–41]; and (ii) two-orbital models without impurities, where the intrinsic coupling between orbitals and the transitions between them generate the Hall-type response [42–44]. In the latter case, any factor influencing interorbital transitions logically affects Hall transport. Notably, SOC emerges as the primary factor, influencing the Fermi surface along the diagonal direction and inducing electron transfer between orbitals in this region [45]. The computational examination of SOC's impact on the polar Kerr effect has shown decreasing in the polar Kerr effect due to SOC [29]. Unlike this claim, Ref. [19] predicted an increase in the Kerr signal due to the presence of SOC. This variation can be ascribed to the utilization of a three-dimensional model characterized by the nodal nature of the tight-binding model (defining the Fermi surface as three slightly warped cylinders along the  $c$ -axis), as well as the gap structure [46,47]. Within this model, SOC induces a pronounced momentum-dependent perpendicularity to the  $\text{RuO}_2$  planes, affecting both orbital and spin characteristics of electronic states near the Fermi level. Significantly, certain regions exhibit a robust SOC effect, while in others, its impact is negligible [48]. Drawing inspiration from the two primary models discussed earlier, which focus on 2D  $p$ -wave chiral pairing, novel models have been suggested to bolster Hall transport phenomena [49–51].

In the present paper, we theoretically study intrinsic Hall response of the superconducting state of  $\text{Sr}_2\text{RuO}_4$ , using the three-orbital model in the presence of SOC. Extending the procedure outlined in Ref. [42], we have determined that the primary contribution to the optical Hall conductivity, and consequently, the polar Kerr effect, emanates from the quasi-1D orbitals, even when considering interorbital interactions within a mixture of two classes and accounting for the rearrangement of orbital hybridization. In other words, at least one of the quasi-1D orbitals needs to have its superconducting time-reversal symmetry broken in order to achieve a suitable Kerr rotation. In the following section, we outline the physical model used to describe the electronic band structure and superconducting ground state. Section III will investigate the dynamical Hall conductivity and calculate the polar Kerr angle based on the most recent suggested superconducting gap functions for  $\text{Sr}_2\text{RuO}_4$ . Finally, the last section provides a short summary and conclusions.

## II. MODEL HAMILTONIAN

Employing the effective three-orbital model that encompasses the  $t_{2g}$  orbital manifold, the Hamiltonian for normal state can be written as follows [52–54]:

$$\mathcal{H}_0 = \sum_{\mathbf{k}} \psi_{\mathbf{k}}^\dagger \hat{\mathcal{H}}(\mathbf{k}) \psi_{\mathbf{k}}, \quad (1)$$

where  $\hat{\mathcal{H}}(\mathbf{k})$  is defined as

$$\hat{\mathcal{H}}(\mathbf{k}) = \begin{pmatrix} \xi_{\mathbf{k}}^{yz} \sigma_0 & \mathbf{g}_{\mathbf{k}} \sigma_0 + i\lambda \sigma_z & -i\lambda \sigma_y \\ \mathbf{g}_{\mathbf{k}} \sigma_0 - i\lambda \sigma_z & \xi_{\mathbf{k}}^{xz} \sigma_0 & i\lambda \sigma_x \\ i\lambda \sigma_y & -i\lambda \sigma_x & \xi_{\mathbf{k}}^{xy} \sigma_0 \end{pmatrix}, \quad (2)$$

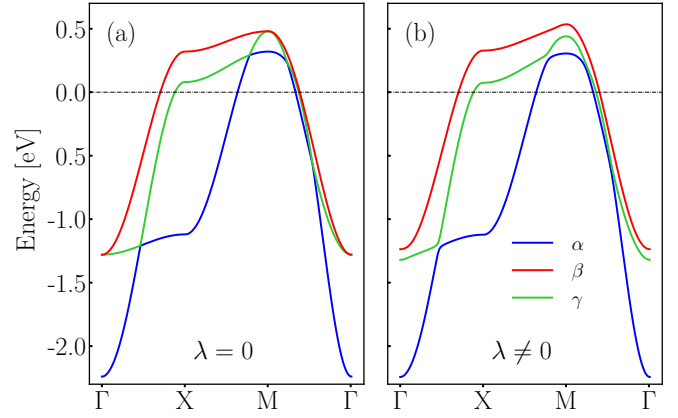


FIG. 1. Energy dispersion along high-symmetry momentum paths  $\Gamma\bar{X}M\Gamma$ , in the absence (a) and presence (b) of spin-orbit coupling.

under the basis  $\psi_{\mathbf{k}}^\dagger = (\phi_{\mathbf{k}\uparrow}^*, \phi_{\mathbf{k}\downarrow}^*)$ , with  $\phi_{\mathbf{k}\sigma}^* = (d_{yz,\mathbf{k}\sigma}^\dagger, d_{xz,\mathbf{k}\sigma}^\dagger, d_{xy,\mathbf{k}\sigma}^\dagger)$ , and  $\sigma_{i=x,y,z}$  denotes the  $2 \times 2$  Pauli matrices in the spin basis. The field operator  $d_{v,\mathbf{k}\sigma}^\dagger$  ( $d_{v,\mathbf{k}\sigma}$ ) creates (annihilates) an electron with momentum  $\mathbf{k}$  and spin  $\sigma$  ( $\bar{\sigma} = -\sigma$ ) at orbital  $v = yz, xz, xy$ . Moreover,  $\lambda$  is the strength of SOC and the electronic dispersions are described by the following tight-binding relations [55]:

$$\begin{aligned} \xi_{\mathbf{k}}^{yz} &= -\mu_1 - 2t_x^{yz} \cos k_x - 2t_y^{yz} \cos k_y, \\ \xi_{\mathbf{k}}^{xz} &= -\mu_1 - 2t_x^{xz} \cos k_x - 2t_y^{xz} \cos k_y, \\ \xi_{\mathbf{k}}^{xy} &= -\mu_2 - 2t_x^{xy} \cos k_x - 2t_y^{xy} \cos k_y - 4t_{xy}^{xy} \cos k_x \cos k_y, \\ \mathbf{g}_{\mathbf{k}} &= -2g \sin k_x \sin k_y, \end{aligned}$$

where  $\mu_{i=1,2}$ ,  $t_{v=x,y,xy}^v$ , and  $g$  represent the chemical potentials, hopping parameters, and the hybridization coefficient, respectively. Moreover, the interorbital coupling  $g$  and hopping integral  $t_{xy}^{xy}$  correspond to the next-nearest neighbors. The tight-binding parameters are set as  $t_x^{xz} = t_y^{yz} = t = 0.4$  eV,  $t_y^{xz} = t_x^{yz} = 0.1t$ ,  $t_x^{xy} = t_y^{xy} = 0.8t$ ,  $t_{xy}^{xy} = 0.3t$ ,  $g = 0.1t$ ,  $\mu_1 = t$ ,  $\mu_2 = 1.1t$  [25]. Figure 1 shows the band structure with and without SOC. Bands  $\alpha$  and  $\beta$  arise from quasi-1D orbitals, while band  $\gamma$  comes from the quasi-2D orbital. The introduction of SOC brings about substantial modifications to the single-particle band structure, particularly at specific high-symmetry points within the Brillouin zone, where multiple bands coincide at the same energy level [56]. Notably, in  $\text{Sr}_2\text{RuO}_4$ , this energy-level degeneracy becomes apparent in the diagonal direction of reciprocal space, leading to the separation of Fermi-surface sheets [48]. This bandsplitting occurs near the Fermi level, and the diagonal region, crucial for the Berry phase, significantly influences the observed anomalous Hall effect [29].

Within the Nambu space  $\psi_{\mathbf{k}}^\dagger = (\phi_{\mathbf{k}\uparrow}^*, \phi_{\mathbf{k}\downarrow}^*, \phi_{-\mathbf{k}\uparrow}, \phi_{-\mathbf{k}\downarrow})$ , the superconducting Hamiltonian can be written as

$$\mathcal{H}_{\text{SC}} = \sum_{\mathbf{k}} \psi_{\mathbf{k}}^\dagger \hat{\mathcal{H}}_{\text{SC}}(\mathbf{k}) \psi_{\mathbf{k}}, \quad (3)$$

where  $\hat{\mathcal{H}}_{\text{SC}}(\mathbf{k})$  is a  $12 \times 12$  tensor defined by

$$\hat{\mathcal{H}}_{\text{SC}}(\mathbf{k}) = \begin{bmatrix} \hat{\mathcal{H}}(\mathbf{k}) & \hat{\Delta}(\mathbf{k}) \\ \hat{\Delta}^\dagger(\mathbf{k}) & -\hat{\mathcal{H}}^*(-\mathbf{k}) \end{bmatrix}, \quad (4)$$

in which the superconducting order parameter is a  $6 \times 6$  anti-diagonal matrix  $\hat{\Delta}(\mathbf{k}) = \Delta(\mathbf{k}) \otimes \sigma_x$ . Here,  $\Delta(\mathbf{k})$  is a  $3 \times 3$  matrix, and we exclusively focus on intra-orbital pairing within a diagonal matrix format, which comprises the following orbital elements  $\Delta_{\mathbf{k}}^v = \Delta_{\mathbf{k}}^{v'} + i\Delta_{\mathbf{k}}^{v''}$ . Note that the multi-orbital (band) structure makes different superconducting gap textures on each orbital (band). Later, we set the most favored forms for the orbital order parameters to calculate intrinsic anomalous Hall transport.

### III. OPTICAL HALL CONDUCTIVITY AND POLAR KERR EFFECT

Within the linear response theory, the dynamical Hall conductivity is given by the following Kubo formula:

$$\sigma^H(\omega) = \frac{1}{2} \lim_{\mathbf{q} \rightarrow 0} [\sigma_{xy}(\mathbf{q}, \omega) - \sigma_{yx}(\mathbf{q}, \omega)], \quad (5)$$

with

$$\sigma_{ij}(\mathbf{q}, \omega) = \frac{i}{\omega} K_{ij}(\mathbf{q}, \omega). \quad (6)$$

Here  $K_{ij}(\mathbf{q}, \omega)$  is the current correlator and is obtained from the analytical continuation,  $i\omega_m \rightarrow \omega + i0^+$ , of its Matsubara counterpart

$$\begin{aligned} & K_{ij}(\mathbf{q}, i\omega_m) \\ &= T \sum_{\mathbf{k}, i\nu_n} \text{Tr}[\hat{\mathcal{J}}_i(\mathbf{k}) \hat{\mathcal{G}}_0(\mathbf{k}, i\nu_n) \hat{\mathcal{J}}_j(\mathbf{k}) \hat{\mathcal{G}}_0(\mathbf{k} + \mathbf{q}, i\nu_n + i\omega_m)], \end{aligned} \quad (7)$$

in which  $\nu_n = 2(n+1)\pi T$ , and  $\omega_m = 2m\pi T$  are Matsubara fermionic and bosonic frequencies, respectively. In the above equation, the bare Green's function in the superconducting state is a  $12 \times 12$  matrix (2 Nambu, 3 orbital, 2 spin degrees of freedom) and is given by

$$\begin{aligned} \hat{\mathcal{G}}_0(\mathbf{k}, i\omega_m) &= [i\omega_m - \hat{\mathcal{H}}_{\text{SC}}(\mathbf{k})]^{-1} \\ &= \begin{bmatrix} \hat{G}_0(\mathbf{k}, i\omega_m) & \hat{F}_0(\mathbf{k}, i\omega_m) \\ \hat{F}_0^\dagger(\mathbf{k}, i\omega_m) & -\hat{G}_0^\dagger(-\mathbf{k}, -i\omega_m) \end{bmatrix}, \end{aligned} \quad (8)$$

in which  $\hat{G}_0(\mathbf{k}, i\omega_m)$  and  $\hat{F}_0(\mathbf{k}, i\omega_m)$  are the normal and anomalous Green's functions, respectively. In Eq. (7), the charge current operator  $\hat{\mathcal{J}}_i(\mathbf{k})$  is defined as

$$\hat{\mathcal{J}}_i(\mathbf{k}) = e\hat{\mathbf{v}}_i(\mathbf{k}) = \hat{f}_i^{(e)}(\mathbf{k}) \oplus \hat{f}_i^{(h)}(\mathbf{k}), \quad (9)$$

wherein

$$\hat{f}_i^{(e)}(\mathbf{k}) = -e\nabla_{k_i} \hat{\mathcal{H}}(\mathbf{k}); \quad \hat{f}_i^{(h)}(\mathbf{k}) = e\nabla_{k_i} (-\hat{\mathcal{H}}^*(-\mathbf{k}))$$

are particle and hole contributions of the charge current operator, respectively. Taking into account the bare current vertex tensor  $\hat{\mathbf{v}}_i(\mathbf{k})$ , and substituting the above terms into Eq. (5), we can show that the Hall conductivity is governed by the following proportionality equation:

$$\sigma^H(\omega) \propto (\mathbf{v}^{xz} - \mathbf{v}^{yz}) \times \mathbf{v}^{xz-yz}, \quad (10)$$

with

$$\mathbf{v}^{xz(yz)} = \partial_{k_x} \xi_{\mathbf{k}}^{xz(yz)} \hat{i} + \partial_{k_y} \xi_{\mathbf{k}}^{xz(yz)} \hat{j};$$

and

$$\mathbf{v}^{xz-yz} = \partial_{k_x} \mathbf{g}_{\mathbf{k}} \hat{i} + \partial_{k_y} \mathbf{g}_{\mathbf{k}} \hat{j},$$

which will end up with different set of the prefactor components of the velocity. Terms including  $\mathbf{v}^{xy}$ , are proportional to  $\lambda^2 g$  that in comparison with  $\mathbf{v}^{yz}$  and  $\mathbf{v}^{xz}$  with dependency as  $g$ , are negligible. Therefore, the dominant terms is related to the prefactors of  $v_x^{yz} v_y^{xz-yz}$ ,  $v_y^{yz} v_x^{xz-yz}$ ,  $v_x^{xz} v_y^{xz-yz}$ , and  $v_y^{xz} v_x^{yz-yz}$  (see Appendix). In fact, these results express that the leading contribution to the Hall-type response originates from the  $d_{yz}$  and  $d_{xz}$  orbitals even in the presence of SOC, which couples the orbital  $d_{xy}$  with these orbitals. Defining  $z = i\nu_n$  and  $z' = i(\omega_m + \nu_n)$  and in accordance with the explanations provided earlier, the dynamical Hall conductivity can be expressed as follows:

$$\begin{aligned} \sigma^H(\omega) &= \frac{2ie^2}{\omega} \sum_{\mathbf{k}} \mathbf{g}_{\mathbf{k}} \Im[\Delta_{\mathbf{k}}^{xz*} \Delta_{\mathbf{k}}^{yz}] \\ &\times [(v_x^{xz} - v_y^{yz}) v_y^{xz-yz} - (v_y^{xz} - v_x^{yz}) v_x^{xz-yz}] \\ &\times \lim_{i\omega_m \rightarrow \omega + i0^+} \left[ T \sum_{i\nu_n} (z^2 - z'^2)(z + z') \right. \\ &\times \frac{(z^2 - E_{\mathbf{k}}^{yz2})(z^2 - E_{\mathbf{k}}^{xz2})(z^2 - E_{\mathbf{k}}^{xy2})^2}{(z^2 - E_{1\mathbf{k}}^2)^2 (z^2 - E_{2\mathbf{k}}^2)^2 (z^2 - E_{3\mathbf{k}}^2)^2} \\ &\left. \times \frac{(z'^2 - E_{\mathbf{k}}^{yz2})(z'^2 - E_{\mathbf{k}}^{xz2})(z'^2 - E_{\mathbf{k}}^{xy2})^2}{(z'^2 - E_{1\mathbf{k}}^2)^2 (z'^2 - E_{2\mathbf{k}}^2)^2 (z'^2 - E_{3\mathbf{k}}^2)^2} \right]. \end{aligned} \quad (11)$$

This expression elucidates the conditions under which the superconducting state may display a nonvanishing Kerr rotation. It implies that there must be a phase difference between the quasi-1D orbitals. Moreover the superconducting state of these two orbitals, in accordance with the two-dimensional feature, must also break the time-reversal symmetry. Additionally, a significant contribution comes from the essential role played by interorbital velocity, which is required for the existence of a nonzero anomalous Hall effect. As a consequence, the quasi-1D orbitals with a  $\mathbf{k}$ -dependent hybridization leads to a nonzero Hall transport. Here we define  $E_{\mathbf{k}}^v = \sqrt{\xi_{\mathbf{k}}^{v2} + |\Delta_{\mathbf{k}}^v|^2}$  for the orbital  $v$ , and the BCS quasiparticle spectra  $E_{i\mathbf{k}}$  ( $i=1-3$ ) can be obtained by rephrasing  $\mathbf{D}(\mathbf{k}, z = i\nu_n) = \det[\mathcal{G}_0^{-1}(\mathbf{k}, i\nu_n)]$ , as

$$\mathbf{D}(\mathbf{k}, z) \propto (z^2 - E_{1\mathbf{k}}^2)^2 (z^2 - E_{2\mathbf{k}}^2)^2 (z^2 - E_{3\mathbf{k}}^2)^2. \quad (12)$$

The minimum of the sum of the quasiparticle spectra occurs at the diagonal zone, where  $k_x = k_y = \pi/2$ . This proximity to the diagonal zone is closely related to orbital hybridization, which plays a pivotal role in determining the frequency dependence of the dynamical Hall-type response in multi-orbital superconductors exhibiting broken time-reversal symmetry. Moreover, the resonance peak that appears at the minimum of the sum of the quasiparticle spectra is affected by the intensity of SOC. The presence of SOC has a notable impact on orbital hybridization, particularly at the point  $(\pi, \pi)$  where the

Fermi surface intersects orbital sheets. Consequently, one can anticipate that this interaction affects the dynamical optical response. However, in the absence of SOC, this minimum shifts to

$$\min[E_{1\mathbf{k}} + E_{3\mathbf{k}}] \approx 2g; \quad E_{2\mathbf{k}} = 0,$$

aligning with the findings of Ref. [57].

The Hall conductivity behavior and other electronic characteristics in the superconducting state are determined by the precise shape of the superconducting gap symmetry. Therefore, to calculate  $\sigma^H(\omega)$ , we need to know the superconducting order parameter. In the case of a two-dimensional square lattice material, the classification of gap symmetries is determined by the irreducible representations (irrep.) of the  $D_{4h}$  group, which encompass extended  $s$ -wave,  $g_{xy(x^2-y^2)}$ ,  $d_{x^2-y^2}$ ,  $d_{xy}$ , and  $p_{x(y)}$ , as elaborated

$$\begin{aligned} A_{1g} : & \quad s' = \cos k_x + \cos k_y, \\ A_{2g} : & \quad g_{xy(x^2-y^2)} = \sin k_x \sin k_y [\cos k_x - \cos k_y], \\ B_{1g} : & \quad d_{x^2-y^2} = \cos k_x - \cos k_y, \\ B_{2g} : & \quad d_{xy} = \sin k_x \sin k_y, \\ E_u : & \quad p_{x(y)} = \sin k_{x(y)}. \end{aligned} \quad (13)$$

In this context, one noteworthy aspect is the capacity to elucidate signs of time-reversal symmetry breaking, prompting our exploration of the following scenarios for superconducting gap momentum dependency [42,58], defined as  $(\Delta_{\mathbf{k}}^{yz}, \Delta_{\mathbf{k}}^{xz})$ :

- (i)  $\Delta_0(i \sin k_y \cos k_x, \sin k_x \cos k_y)$
- (ii)  $\Delta_0(\cos k_x - i \cos k_x, \cos k_y + i \cos k_y)$
- (iii)  $\Delta_0(\cos k_x + i \sin k_y \cos k_x, \cos k_y + i \sin k_x \cos k_y)$ ,

for  $p + ip$ ,  $s' + id$ , and  $s' + ip$ , respectively. Moreover, we set the pairing on the  $d_{xy}$  orbital as [6,59,60]

$$\Delta_{\mathbf{k}}^{xy} = \Delta'_0(\cos k_x - \cos k_y)(1 + i \sin k_x \sin k_y). \quad (15)$$

In Fig. 2, we illustrate the results for the dynamical Hall conductivity at zero temperature  $\sigma^H(\omega)$  across three different strengths of SOC. The finite values of SOC are chosen as  $\lambda = g/2$  [61] and  $\lambda = g$  [32,48], and we set  $\Delta'_0 = 2\Delta_0 = 0.5$  meV [42]. In the lower panel, we observe  $\Im\sigma^H(\omega)$ , which characterizes the absorption spectrum. In the absence of SOC for all pairings, the initiation of absorption processes, arising from orbital hopping between  $d_{yz}$  and  $d_{xz}$  orbitals, manifests at the interorbital interaction and peaks at the minimum point in the sum of the two lowest BCS quasiparticle spectra in the diagonal region, i.e.,  $2g$ . Incorporating SOC results in a notable shift of both the onset and resonance peak toward higher frequencies. This shift may be related to the reconfiguration of hybridization between the quasi-1D orbitals, the introduction of transitions involving the quasi-2D orbital with the quasi-1D orbitals, and the energy splitting in regions characterized by degenerate  $t_{2g}$  bands. In fact, the frequency region  $2\Delta_0 \lesssim \omega \lesssim 2g + \lambda$  corresponds to interorbital hoppings, which can arise from either interorbital interactions or SOC. The main peaks in this region are attributed to near degeneracies (along the diagonal zone) between orbitals in the quasiparticle band structure and the orbital mixing. The positive feature seen

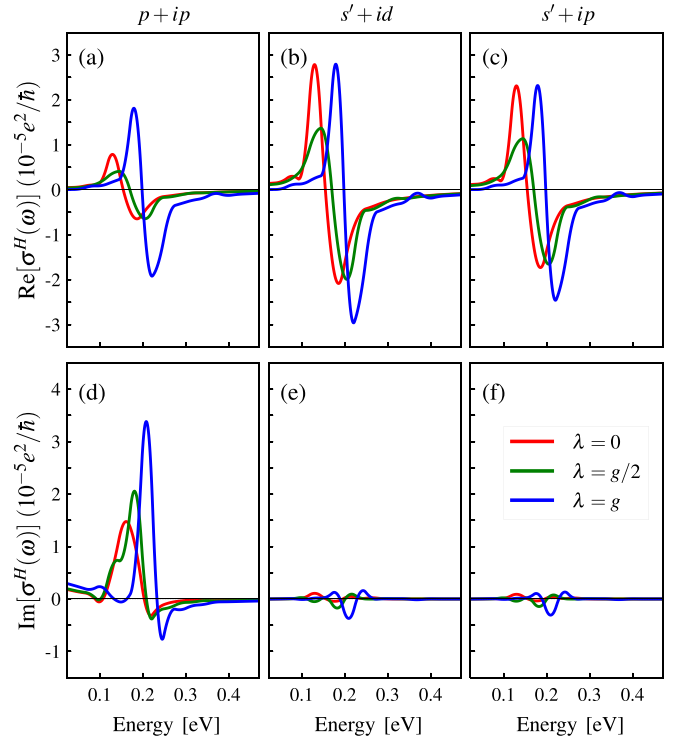


FIG. 2. [(a)–(c)] Plotting the real parts and [(d)–(f)] imaginary parts of the dynamical Hall conductivity  $\sigma^H(\omega)$  vs photon energy at zero temperature for various quasi-1D pairings:  $p + ip$ ,  $s' + id$ , and  $s' + ip$ , with the  $d + ig$  pairing for quasi-2D orbital, considering values of the spin-orbit coupling:  $\lambda = 0$  (red),  $\lambda = g/2$  (green), and  $\lambda = g$  (blue).

at frequencies  $\omega \lesssim 0.1$  ( $\omega \lesssim 0.15$ ), as well as the negative features around 0.1 eV and 0.2 eV (0.15 eV and 0.25 eV) for  $\lambda = 0$  ( $\lambda \approx g$ ), can be assigned to the appearance of the  $d_{xy}$  orbital and its hopping with the quasi-1D orbitals by comparing Figs. 2(d)–2(f) with the findings in Ref. [42]. Additionally, it is worth noting that the various pairings exhibit distinct resonance peak intensities and spectral weights, likely associated to their unique pairing characteristics. In the case of nonchiral pairings, the absorption spectrum tends to be smaller compared to the chiral case. A substantial reduction in spectral weight occurs at higher frequencies, approximately  $\omega \gtrsim 0.4$  eV, which corresponds to associated with strongly correlated electronic limit.

Utilizing the dynamical Hall conductivity and following the established formalism of Kerr rotation one can obtain the polar Kerr angle as

$$\theta^{\text{Kerr}}(\omega) = \frac{4\pi}{\omega d} \Im[\sigma^H(\omega)\varphi(\omega)], \quad (16)$$

where  $d = 6.8$  Å is the interlayer distance [38], and

$$\varphi(\omega) = [n(\omega)[n(\omega)^2 - 1]]^{-1}.$$

Here  $n(\omega) = \sqrt{\epsilon_\infty + (4\pi i/\omega)\sigma(\omega)}$  denotes the refraction index defined by the dynamical Drude model,  $\sigma(\omega) = \sigma_0/(1 - i\omega\tau)$ , where  $\sigma_0$  is the static Drude conductivity with relaxation time  $\tau^{-1} = \gamma_{\text{Scatt}} = 0.4$  eV, and  $\epsilon_\infty = 10$  refers to the background dielectric tensor. Notice that Kerr angle strongly depends on the quasiparticle scattering rate  $\gamma_{\text{Scatt}}$  [38,39].

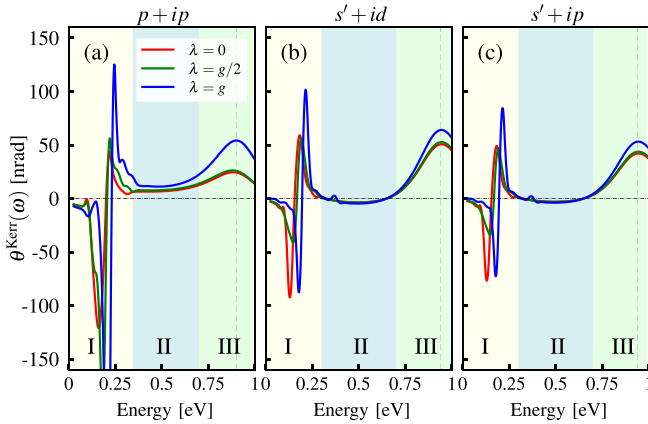


FIG. 3. Plotting the Kerr rotation angle (in unit of nanoradian) vs photon energy for three pairing symmetries:  $p + ip$ ,  $s' + id$ , and  $s' + ip$ , for three values of spin-orbit coupling:  $\lambda = 0$ ,  $\lambda = g/2$ , and  $\lambda = g$ . We can roughly categorize the behavior of the Kerr rotation angle into three distinct regimes: I, II, and III. The region I represents interorbital transitions, and the vertical dashed line indicates the maximum of angle in the region III.

The results of Kerr rotation angle versus the photon energy are shown in Fig. 3, covering different strengths of SOC and for pairing symmetries: (a)  $p + ip$ , (b)  $s' + id$ , and (c)  $s' + ip$ . In a qualitative sense, we can delineate three primary regions labeled as I, II, and III, each represented by distinct colors. The region I, encompassing frequencies  $\omega \lesssim 0.3$  eV, reveals a complex structure with the resonant enhancements which are associated with interorbital transitions. In the intermediate frequency range (region II), the Kerr rotation angle exhibits a distinctive flat-like behavior. The variation in this region can be attributed to the fact that the primary contribution to  $\theta^{\text{Kerr}}(\omega)$  for nonchiral pairings arises from the real part of  $\sigma^H(\omega)$  in the strongly correlated system limit. In contrast, for the chiral pairing  $p + ip$ , both the real and imaginary parts of  $\sigma^H(\omega)$  are of similar magnitude, resulting in comparable contributions to  $\theta^{\text{Kerr}}(\omega)$ . On the other hand, region III shows a hump that corresponds to the situation where the spectra are dominated by a strong magneto-optical response at  $\omega < \omega_{\text{edge}}$  for chiral pairing and at  $\omega > \omega_{\text{edge}}$  for nonchiral pairings, respectively. Here  $\omega_{\text{edge}} = \omega_p / \sqrt{\epsilon_\infty}$  is the frequency of the plasma edge, and  $\omega_p$  is the plasma frequency and we set it as  $\omega_p = 2.9$  eV [38,42]. The behavior of the Kerr spectra suggests a broadening of the optical response and a sensitivity to pairing in the intermediate region, especially in proximity to the plasma edge [57]. Interestingly, in region III, the peak of the Kerr angle shifts towards higher energy for the nonchiral pairings. In fact, for the nonchiral pairings, the Kerr angle is primarily dominated by the real part of the frequency-dependent Hall conductivity; however, for the chiral pairing  $p + ip$ , the Kerr angle receives contributions from both the real and imaginary parts, as indicated in Table I.

Notably, the inclusion of SOC leads to an enhancement in the Kerr angle. This effect could be attributed to the introduction of spin magnetic order, which contributes to the observed finite Kerr signal in a spin system. In this framework,

TABLE I. Comparing the results obtained for maximum Kerr rotation (at region III) for three considered pairing symmetries:  $p + ip$ ,  $s' + id$ , and  $s' + ip$ . Polar Kerr spectrum is peaked at  $\omega \approx 0.85$  eV and  $\omega \approx 0.95$  eV for the chiral and nonchiral pairings, respectively; indicating by the vertical dashed lines in Fig. 3. Each dataset within individual cells corresponds to the calculated results for  $\lambda = 0$ ,  $\lambda = g/2$ , and  $\lambda = g$ , respectively.

Pairings	$\theta^{\text{Kerr}}$ (nrad)	$\Im[\sigma^H](10^{-8}e^2/\hbar)$	$\Re[\sigma^H](10^{-8}e^2/\hbar)$
$p + ip$	25, 26, 54	-6.2, -7, -10	-7.3, -7.6, -18.4
$s' + id$	51, 53, 64	0.04, 0.042, 0.05	-18.4, -19, -23.2
$s' + ip$	42, 44, 53	0.033, 0.035, 0.043	-15.2, -15, -19.3

magnetic order pertains to the transitions occurring between orbitals, in which the magnetic orbital (spin) order describes electronic transitions between orbitals without (with) considering spin [45]. Since these transitions between orbitals exclusively occurs among quasi-1D orbitals, the quasi-2D orbital does not partake in the development of the orbital magnetic moment [42,46]. Spin magnetic order emerges due to the presence of SOC, resulting in the interplay among three orbitals. However, as elucidated in our findings, the primary contribution to the Hall conductivity comes from quasi-1D orbitals. Consequently, SOC induces more transitions between quasi-1D orbitals, providing an explanation for the amplified Kerr signal.

At the end, in comparison with existing experimental findings [62], where  $\theta_{\text{Exp}}^{\text{Kerr}} \approx 65$  nrad was measured at  $\omega = 0.8$  eV, the results obtained for all three pairings appear to be in reasonable agreement, particularly for the chiral order parameter.

#### IV. SUMMARY

We have presented a detailed theoretical study of the intrinsic Kerr response for the three-orbital model in the presence of spin-orbit coupling  $\lambda$ , as an application model for  $\text{Sr}_2\text{RuO}_4$  superconductor. Our investigation has unveiled that the spontaneous Hall transport, resulting in a nonzero Kerr angle and finite Berry curvature, is primarily instigated by the quasi-1D orbitals  $d_{xz}$  and  $d_{yz}$  with a interorbital coupling  $g$ . We have demonstrated that the terms associated with the quasi-1D orbitals primarily influence the results, as they are directly proportional to  $g$ . In contrast, the contribution of the orbital  $d_{xy}$  to the optical Hall response are expressed as a proportionality to  $\lambda^2 g$ , and can be neglected. As a result, the absence of edge currents can be rationalized by considering the  $d_{xz}$  and  $d_{yz}$  orbitals as the primary active components. This choice arises because the components of the pairings in these orbitals are nearly decoupled, except in small regions of  $\mathbf{k}$  space where the Fermi surfaces closely intersect. Consequently, this scenario leads to a substantial reduction in edge currents. The SOC plays a pivotal role in amplifying the intensity of the resonance peak, particularly when the frequency of electromagnetic radiation aligns with the characteristic scale of hybridization. This heightened hybridization, in turn, leads to a remarkable enhancement of the Kerr angle for possible pairing states characterized by the breaking of

time-reversal symmetry. This enhancement can be attributed to the incorporation of contributions from spin magnetic order into the optical Hall response and the influence of Berry curvature.

### ACKNOWLEDGMENT

We acknowledge Thomas Scaffidi and Yunkyu Bang for the helpful discussions. A.A. acknowledges the financial support from the German Research Foundation within the bilateral NSFC-DFG Project No. ER 463/14-1.

### APPENDIX

Here, we offer a synopsis of the numerator prefactors associated with each term in Eq. (11), categorized by velocity type, while neglecting terms of order  $\mathcal{O}\lambda^2g$ . For the terms that

include  $v_x^{yz}v_y^{xz-yz}$  and  $v_y^{yz}v_x^{xz-yz}$ , we can write

$$\begin{aligned} & 4g_{\mathbf{k}}(z-z')(z+z')^2\Im[\Delta_{\mathbf{k}}^{xz*}\Delta_{\mathbf{k}}^{yz}] \\ & \times (z^2 - E_{\mathbf{k}}^{xz2})(z^2 - E_{\mathbf{k}}^{yz2})(z^2 - E_{\mathbf{k}}^{xy2})^2 \\ & \times (z'^2 - E_{\mathbf{k}}^{xz2})(z'^2 - E_{\mathbf{k}}^{yz2})(z'^2 - E_{\mathbf{k}}^{xy2})^2 + \mathcal{O}\lambda^2g, \end{aligned}$$

and for the terms that include  $v_x^{xz}v_y^{xz-yz}$  and  $v_y^{xz}v_x^{xz-yz}$ , we have

$$\begin{aligned} & -4g_{\mathbf{k}}(z-z')(z+z')^2\Im[\Delta_{\mathbf{k}}^{xz*}\Delta_{\mathbf{k}}^{yz}] \\ & \times (z^2 - E_{\mathbf{k}}^{yz2})(z^2 - E_{\mathbf{k}}^{xz2})(z^2 - E_{\mathbf{k}}^{xy2})^2 \\ & \times (z'^2 - E_{\mathbf{k}}^{yz2})(z'^2 - E_{\mathbf{k}}^{xz2})(z'^2 - E_{\mathbf{k}}^{xy2})^2 + \mathcal{O}\lambda^2g. \end{aligned}$$

Furthermore, the inclusion of the following terms:  $v_x^{yz}v_y^{xy}$ ,  $v_y^{yz}v_x^{xy}$ ,  $v_x^{xz}v_y^{xy}$ ,  $v_y^{xz}v_x^{xy}$ ,  $v_x^{xy}v_y^{xz-yz}$ , and  $v_y^{xy}v_x^{xz-yz}$ , all are proportional to  $\mathcal{O}\lambda^2g$ , making them negligible. For the rest of the components, these coefficients vanish.

- 
- [1] S. Benhabib, C. Lupien, I. Paul, L. Berges, M. Dion, M. Nardone, A. Zitouni, Z. Q. Mao, Y. Maeno, A. Georges *et al.*, Ultrasound evidence for a two-component superconducting order parameter in  $\text{Sr}_2\text{RuO}_4$ , *Nat. Phys.* **17**, 194 (2021).
- [2] A. Chronister, A. Pustogow, N. Kikugawa, D. A. Sokolov, F. Jerzembeck, C. W. Hicks, A. P. Mackenzie, E. D. Bauer, and S. E. Brown, Evidence for even parity unconventional superconductivity in  $\text{Sr}_2\text{RuO}_4$ , *Proc. Natl. Acad. Sci. USA* **118**, e2025313118 (2021).
- [3] S. Ghosh, A. Shekhter, F. Jerzembeck, N. Kikugawa, D. A. Sokolov, M. Brando, A. P. Mackenzie, C. W. Hicks, and B. J. Ramshaw, Thermodynamic evidence for a two-component superconducting order parameter in  $\text{Sr}_2\text{RuO}_4$ , *Nat. Phys.* **17**, 199 (2021).
- [4] V. Grinenko, S. Ghosh, R. Sarkar, J.-C. Orain, A. Nikitin, M. Elender, D. Das, Z. Guguchia, F. Brückner, M. E. Barber *et al.*, Split superconducting and time-reversal symmetry-breaking transitions in  $\text{Sr}_2\text{RuO}_4$  under stress, *Nat. Phys.* **17**, 748 (2021).
- [5] V. Grinenko, D. Weston, F. Cagliaris, C. Wuttke, C. Hess, T. Gottschall, I. Maccari, D. Gorbunov, S. Zherlitsyn, J. Wosnitzer *et al.*, State with spontaneously broken time-reversal symmetry above the superconducting phase transition, *Nat. Phys.* **17**, 1254 (2021).
- [6] S. A. Kivelson, A. C. Yuan, B. Ramshaw, and R. Thomale, A proposal for reconciling diverse experiments on the superconducting state in  $\text{Sr}_2\text{RuO}_4$ , *npj Quantum Mater.* **5**, 43 (2020).
- [7] A. T. Rømer, P. J. Hirschfeld, and B. M. Andersen, Superconducting state of  $\text{Sr}_2\text{RuO}_4$  in the presence of longer-range coulomb interactions, *Phys. Rev. B* **104**, 064507 (2021).
- [8] S. Bhattacharyya, A. Kreisel, X. Kong, T. Berlijn, A. T. Rømer, B. M. Andersen, and P. J. Hirschfeld, Superconducting gap symmetry from Bogoliubov quasiparticle interference analysis on  $\text{Sr}_2\text{RuO}_4$ , *Phys. Rev. B* **107**, 144505 (2023).
- [9] S. Käser, H. U. R. Strand, N. Wentzell, A. Georges, O. Parcollet, and P. Hansmann, Interorbital singlet pairing in  $\text{Sr}_2\text{RuO}_4$ : A Hund's superconductor, *Phys. Rev. B* **105**, 155101 (2022).
- [10] S. Ikegaya, K. Yada, Y. Tanaka, S. Kashiwaya, Y. Asano, and D. Manske, Identification of spin-triplet superconductivity through a helical-chiral phase transition in  $\text{Sr}_2\text{RuO}_4$  thin films, *Phys. Rev. B* **101**, 220501(R) (2020).
- [11] O. Gingras, N. Allaglo, R. Nourafkan, M. Côté, and A.-M. S. Tremblay, Superconductivity in correlated multi-orbital systems with spin-orbit coupling: Coexistence of even- and odd-frequency pairing, and the case of  $\text{Sr}_2\text{RuO}_4$ , *Phys. Rev. B* **106**, 064513 (2022).
- [12] G. Wagner, H. S. Røising, F. Flicker, and S. H. Simon, Microscopic Ginzburg-Landau theory and singlet ordering in  $\text{Sr}_2\text{RuO}_4$ , *Phys. Rev. B* **104**, 134506 (2021).
- [13] A. W. Lindquist and H.-Y. Kee, Distinct reduction of knight shift in superconducting state of  $\text{Sr}_2\text{RuO}_4$  under uniaxial strain, *Phys. Rev. Res.* **2**, 032055(R) (2020).
- [14] A. W. Lindquist and H.-Y. Kee, Reconciling the  $\pi$  phase shift in Josephson junction experiments with even-parity superconductivity in  $\text{Sr}_2\text{RuO}_4$ , *Phys. Rev. B* **107**, 014506 (2023).
- [15] R. Willa, M. Hecker, R. M. Fernandes, and J. Schmalian, Inhomogeneous time-reversal symmetry breaking in  $\text{Sr}_2\text{RuO}_4$ , *Phys. Rev. B* **104**, 024511 (2021).
- [16] A. T. Rømer, T. A. Maier, A. Kreisel, P. J. Hirschfeld, and B. M. Andersen, Leading superconducting instabilities in three-dimensional models for  $\text{Sr}_2\text{RuO}_4$ , *Phys. Rev. Res.* **4**, 033011 (2022).
- [17] T. M. Rice and M. Sigrist,  $\text{Sr}_2\text{RuO}_4$ : An electronic analogue of  $^3\text{He}$ ? *J. Phys.: Condens. Matter* **7**, L643 (1995).
- [18] G. M. Luke, Y. Fudamoto, K. M. Kojima, M. I. Larkin, J. Merrin, B. Nachumi, Y. J. Uemura, Y. Maeno, Z. Q. Mao, Y. Mori *et al.*, Time-reversal symmetry-breaking superconductivity in  $\text{Sr}_2\text{RuO}_4$ , *Nature (London)* **394**, 558 (1998).
- [19] J. Xia, Y. Maeno, P. T. Beyersdorf, M. M. Fejer, and A. Kapitulnik, High resolution polar Kerr effect measurements of  $\text{Sr}_2\text{RuO}_4$ : Evidence for broken time-reversal symmetry in the superconducting state, *Phys. Rev. Lett.* **97**, 167002 (2006).
- [20] T. Scaffidi and S. H. Simon, Large Chern number and edge currents in  $\text{Sr}_2\text{RuO}_4$ , *Phys. Rev. Lett.* **115**, 087003 (2015).
- [21] C. W. Hicks, D. O. Brodsky, E. A. Yelland, A. S. Gibbs, J. A. Bruin, M. E. Barber, S. D. Edkins, K. Nishimura, S. Yonezawa,

- Y. Maeno *et al.*, Strong increase of  $T_c$  of  $\text{Sr}_2\text{RuO}_4$  under both tensile and compressive strain, *Science* **344**, 283 (2014).
- [22] A. Steppke, L. Zhao, M. E. Barber, T. Scaffidi, F. Jerzembeck, H. Rosner, A. S. Gibbs, Y. Maeno, S. H. Simon, A. P. Mackenzie, and C. W. Hicks, Strong peak in  $T_c$  of  $\text{Sr}_2\text{RuO}_4$  under uniaxial pressure, *Science* **355**, eaaf9398 (2017).
- [23] K. Ishida, M. Manago, K. Kinjo, and Y. Maeno, Reduction of the  $^{17}\text{O}$  Knight shift in the superconducting state and the heat-up effect by NMR pulses on  $\text{Sr}_2\text{RuO}_4$ , *J. Phys. Soc. Jpn.* **89**, 034712 (2020).
- [24] D. F. Agterberg, T. M. Rice, and M. Sigrist, Orbital dependent superconductivity in  $\text{Sr}_2\text{RuO}_4$ , *Phys. Rev. Lett.* **78**, 3374 (1997).
- [25] S. Cobo, F. Ahn, I. Eremin, and A. Akbari, Anisotropic spin fluctuations in  $\text{Sr}_2\text{RuO}_4$ : Role of spin-orbit coupling and induced strain, *Phys. Rev. B* **94**, 224507 (2016).
- [26] M. E. Barber, A. S. Gibbs, Y. Maeno, A. P. Mackenzie, and C. W. Hicks, Resistivity in the vicinity of a van Hove singularity:  $\text{Sr}_2\text{RuO}_4$  under uniaxial pressure, *Phys. Rev. Lett.* **120**, 076602 (2018).
- [27] Y. Yu, S. Brown, S. Raghu, and K. Yang, Critical temperature  $T_c$  and Pauli limited critical field of  $\text{Sr}_2\text{RuO}_4$ : Uniaxial strain dependence, *Phys. Rev. B* **102**, 014509 (2020).
- [28] B. Kim, S. Khmelevskiy, C. Franchini, and I. I. Mazin, Suppressed fluctuations as the origin of the static magnetic order in strained  $\text{Sr}_2\text{RuO}_4$ , *Phys. Rev. Lett.* **130**, 026702 (2023).
- [29] J. Robbins, J. F. Annett, and M. Gradhand, Effect of spin-orbit coupling on the polar Kerr effect in  $\text{Sr}_2\text{RuO}_4$ , *Phys. Rev. B* **96**, 144503 (2017).
- [30] M. Gradhand and J. F. Annett, The Berry curvature of the Bogoliubov quasiparticle Bloch states in the unconventional superconductor  $\text{Sr}_2\text{RuO}_4$ , *J. Phys.: Condens. Matter* **26**, 274205 (2014).
- [31] Y. Sidis, M. Braden, P. Bourges, B. Hennion, S. NishiZaki, Y. Maeno, and Y. Mori, Evidence for incommensurate spin fluctuations in  $\text{Sr}_2\text{RuO}_4$ , *Phys. Rev. Lett.* **83**, 3320 (1999).
- [32] S. Raghu, A. Kapitulnik, and S. A. Kivelson, Hidden quasi-one-dimensional superconductivity in  $\text{Sr}_2\text{RuO}_4$ , *Phys. Rev. Lett.* **105**, 136401 (2010).
- [33] I. A. Firmo, S. Lederer, C. Lupien, A. P. Mackenzie, J. C. Davis, and S. A. Kivelson, Evidence from tunneling spectroscopy for a quasi-one-dimensional origin of superconductivity in  $\text{Sr}_2\text{RuO}_4$ , *Phys. Rev. B* **88**, 134521 (2013).
- [34] K. Deguchi, Z. Q. Mao, H. Yaguchi, and Y. Maeno, Gap structure of the spin-triplet superconductor  $\text{Sr}_2\text{RuO}_4$  determined from the field-orientation dependence of the specific heat, *Phys. Rev. Lett.* **92**, 047002 (2004).
- [35] P. G. Björnsson, Y. Maeno, M. E. Huber, and K. A. Moler, Scanning magnetic imaging of  $\text{Sr}_2\text{RuO}_4$ , *Phys. Rev. B* **72**, 012504 (2005).
- [36] J. R. Kirtley, C. Kallin, C. W. Hicks, E.-A. Kim, Y. Liu, K. A. Moler, Y. Maeno, and K. D. Nelson, Upper limit on spontaneous supercurrents in  $\text{Sr}_2\text{RuO}_4$ , *Phys. Rev. B* **76**, 014526 (2007).
- [37] C. W. Hicks, J. R. Kirtley, T. M. Lippman, N. C. Koshnick, M. E. Huber, Y. Maeno, W. M. Yuhasz, M. B. Maple, and K. A. Moler, Limits on superconductivity-related magnetization in  $\text{Sr}_2\text{RuO}_4$  and  $\text{PrOs}_4\text{Sb}_{12}$  from scanning squid microscopy, *Phys. Rev. B* **81**, 214501 (2010).
- [38] R. M. Lutchyn, P. Nagornykh, and V. M. Yakovenko, Frequency and temperature dependence of the anomalous ac Hall conductivity in a chiral  $p_x + ip_y$  superconductor with impurities, *Phys. Rev. B* **80**, 104508 (2009).
- [39] J. Goryo, Impurity-induced polar Kerr effect in a chiral  $p$ -wave superconductor, *Phys. Rev. B* **78**, 060501(R) (2008).
- [40] W. Kim, F. Marsiglio, and C. S. Ting, Hall conductivity of a spin-triplet superconductor, *Phys. Rev. Lett.* **100**, 227003 (2008).
- [41] E. J. König and A. Levchenko, Kerr effect from diffractive skew scattering in chiral  $p_x \pm ip_y$  superconductors, *Phys. Rev. Lett.* **118**, 027001 (2017).
- [42] E. Taylor and C. Kallin, Intrinsic Hall effect in a multiband chiral superconductor in the absence of an external magnetic field, *Phys. Rev. Lett.* **108**, 157001 (2012).
- [43] K. I. Wysokiński, J. F. Annett, and B. L. Györfy, Intrinsic optical dichroism in the chiral superconducting state of  $\text{Sr}_2\text{RuO}_4$ , *Phys. Rev. Lett.* **108**, 077004 (2012).
- [44] M. D. E. Denys and P. M. R. Brydon, Origin of the anomalous Hall effect in two-band chiral superconductors, *Phys. Rev. B* **103**, 094503 (2021).
- [45] H. Kontani, T. Tanaka, D. S. Hirashima, K. Yamada, and J. Inoue, Giant intrinsic spin and orbital Hall effects in  $\text{Sr}_2\text{MO}_4$  ( $M = \text{Ru}, \text{Rh}, \text{Mo}$ ), *Phys. Rev. Lett.* **100**, 096601 (2008).
- [46] J. F. Annett, B. L. Györfy, and K. I. Wysokiński, Orbital magnetic moment of a chiral  $p$ -wave superconductor, *New J. Phys.* **11**, 055063 (2009).
- [47] M. Gradhand, K. I. Wysokiński, J. F. Annett, and B. L. Györfy, Kerr rotation in the unconventional superconductor  $\text{Sr}_2\text{RuO}_4$ , *Phys. Rev. B* **88**, 094504 (2013).
- [48] M. W. Haverkort, I. S. Elfimov, L. H. Tjeng, G. A. Sawatzky, and A. Damascelli, Strong spin-orbit coupling effects on the Fermi surface of  $\text{Sr}_2\text{RuO}_4$  and  $\text{Sr}_2\text{RhO}_4$ , *Phys. Rev. Lett.* **101**, 026406 (2008).
- [49] J.-L. Zhang, Y. Li, W. Huang, and F.-C. Zhang, Hidden anomalous Hall effect in  $\text{Sr}_2\text{RuO}_4$  with chiral superconductivity dominated by the Ru  $d_{xy}$  orbital, *Phys. Rev. B* **102**, 180509(R) (2020).
- [50] H.-T. Liu, W. Chen, and W. Huang, Impact of random impurities on the anomalous Hall effect in chiral superconductors, *Phys. Rev. B* **107**, 224517 (2023).
- [51] J.-L. Zhang, W. Chen, H.-T. Liu, Y. Li, Z. Wang, and W. Huang, Quantum-geometry-induced anomalous Hall effect in non-unitary superconductors and application to  $\text{Sr}_2\text{RuO}_4$ , [arXiv:2309.14448](https://arxiv.org/abs/2309.14448).
- [52] A. Ramires and M. Sigrist, Identifying detrimental effects for multiorbital superconductivity: Application to  $\text{Sr}_2\text{RuO}_4$ , *Phys. Rev. B* **94**, 104501 (2016).
- [53] A. Ramires and M. Sigrist, A note on the upper critical field of  $\text{Sr}_2\text{RuO}_4$  under strain, *J. Phys.: Conf. Ser.* **807**, 052011 (2017).
- [54] Z. Wang, X. Wang, and C. Kallin, Spin-orbit coupling and spin-triplet pairing symmetry in  $\text{Sr}_2\text{RuO}_4$ , *Phys. Rev. B* **101**, 064507 (2020).
- [55] A. Akbari and P. Thalmeier, Multiorbital and hybridization effects in the quasiparticle interference of the triplet superconductor  $\text{Sr}_2\text{RuO}_4$ , *Phys. Rev. B* **88**, 134519 (2013).
- [56] H. Suzuki, L. Wang, J. Bertinshaw, H. U. R. Strand, S. Käser, M. Krautloher, Z. Yang, N. Wentzell, O. Parcollet, F. Jerzembeck *et al.*, Distinct spin and orbital dynamics in  $\text{Sr}_2\text{RuO}_4$ , *Nat. Commun.* **14**, 7042 (2023).

- [57] E. Taylor and C. Kallin, Anomalous Hall conductivity of clean  $\text{Sr}_2\text{RuO}_4$  at finite temperatures, *J. Phys.: Conf. Ser.* **449**, 012036 (2013).
- [58] T. Scaffidi, Degeneracy between even- and odd-parity superconductivity in the quasi-one-dimensional Hubbard model and implications for  $\text{Sr}_2\text{RuO}_4$ , *Phys. Rev. B* **107**, 014505 (2023).
- [59] G. Palle, C. Hicks, R. Valentí, Z. Hu, Y.-S. Li, A. Rost, M. Nicklas, A. P. Mackenzie, and J. Schmalian, Constraints on the superconducting state of  $\text{Sr}_2\text{RuO}_4$  from elastocaloric measurements, *Phys. Rev. B* **108**, 094516 (2023).
- [60] X. Wang, Z. Wang, and C. Kallin, Higher angular momentum pairing states in  $\text{Sr}_2\text{RuO}_4$  in the presence of longer-range interactions, *Phys. Rev. B* **106**, 134512 (2022).
- [61] Y. Yanase and M. Ogata, Microscopic identification of the D-vector in triplet superconductor  $\text{Sr}_2\text{RuO}_4$ , *J. Phys. Soc. Jpn.* **72**, 673 (2003).
- [62] T. Katsufuji, M. Kasai, and Y. Tokura, In-plane and out-of-plane optical spectra of  $\text{Sr}_2\text{RuO}_4$ , *Phys. Rev. Lett.* **76**, 126 (1996).